Nano Research 2013, 6(9): 652–670
DOI 10.1007/s12274-013-0341-7
Research Article

ISSN 1998-0124
CN 11-5974/O4

Highly reactive, flexible yet green Se precursor for metal selenide nanocrystals: Se–octadecene suspension (Se–SUS)

Chaodan Pu, Jianhai Zhou, Runchen Lai, Yuan Niu, Wennuan Nan, and Xiaogang Peng (✉)

Center for Chemistry of Novel & High-Performance Materials, and Department of Chemistry, Zhejiang University, Hangzhou 310027, China

Received: 31 May 2013
Accepted: 2 June 2013

KEYWORDS
selenium precursor, selenium suspension, metal selenide nanocrystals

ABSTRACT

A suspension of fine selenium (Se) powder (100 or 200 mesh) in octadecene (Se–SUS) has proven to be a high-performance, versatile, convenient, reproducible, yet green Se precursor. The advantages of Se–SUS arise from its highly reactive chemical nature and flexibility. These two features made it possible to carry out the synthesis of high quality metal selenide nanocrystals with diverse compositions and structures, including binary, core/shell, transition metal doped, and complex composition nanocrystals. These successes further demonstrated that Se–SUS is a powerful Se precursor for solving a few long-standing challenges in the synthesis of high quality selenide nanocrystals. For instance, Se–SUS was successfully employed as a Se precursor for shell growth in high quality core/shell nanocrystals to replace expensive and highly toxic precursors, such as Se–phosphine and bis-trimethylsilyl selenide, with greatly lowered epitaxial temperatures (as low as 150 ˚C) to avoid alloying. As another example, Se–SUS enabled "co-nucleation doping" as a means of preparing high quality Mn doped ZnSe nanocrystals with pure, stable, and highly efficient dopant fluorescence.

1 Introduction

Synthetic chemistry of colloidal semiconductor nanocrystals [1, 2] has been become an important field in chemistry and materials science because of the interesting size-dependent properties and solution-based processing chemistry of these materials. Among all types of semiconductor nanocrystals, metal selenides are the most pursued class in the field. For example, CdSe nanocrystals in the quantum confinement size regime (quantum dots) are often regarded as the model system for all semiconductor nanocrystals after the landmark publication by Bawendi's group in 1993 [3]. ZnSe nanocrystals play an essential role in developing transition metal doped semiconductor nanocrystals [4, 5] as non-cadmium fluorescent nanocrystals. Simultaneously, these transition metal doped ZnSe nanocrystals have been actively explored as

Address correspondence to xpeng@zju.edu.cn

spintronics materials [6, 7]. Recently, metal selenide nanocrystals have been intensively investigated as promising thermal electric materials [8–10]. In the field of solar cells, metal selenides—including binary [11] and complex [12] selenides—are also being actively investigated. Despite this great interest, the synthetic chemistry of metal selenide nanocrystals is still under-developed, mostly because of the lack of a high-performance, versatile, yet green Se precursor.

The advancement in the synthetic chemistry of colloidal nanocrystals in the past 20 years is largely associated with metal chalcogenide nanocrystals, especially metal selenide nanocrystals. On the basis of the landmark publication by Bawendi's group in 1993 [3], we replaced dimethyl cadmium used in the Bawendi synthesis by CdO [13] as well as Cd carboxylates [14] in 2001, but toxic and expensive Se–organophosphine complexes were still required as the Se precursor. In 2002, a synthetic scheme for CdS nanocrystals only using cadmium oxide (CdO), elemental S powder, and octadecene (ODE) was reported [15]. This green S precursor (elemental S dissolved in ODE) has subsequently proven to be rather versatile for the synthesis of other types of sulfide nanocrystals. However, replacement of elemental S by elemental Se was unsuccessful because Se powder is not soluble in ODE at room temperature [15]. Since 2005, replacements for the Se–organophosphine precursor have been reported quite frequently in the literature, including pre-reacting elemental Se with alkanes [16], a non-injection approach involving mixing elemental Se powder and Cd fatty acid salts in ODE at room temperature [17], dissolving elemental Se in ODE using a long heating time to form Se–ODE solution [18], mixing SeO_2 with ODE [19, 20], and, recently, dissolving elemental Se in ODE in the presence of either $NaBH_4$ [21] or an aliphatic thiol [22]. Each of these approaches apparently has its own advantages but none of them has been accepted as the standard method. Among all these alternatives, the non-injection approach [17] seemed to be the simplest one and the Se–ODE solution approach [18] is the most developed one at present.

Cao's group reported the synthesis of CdSe nanocrystals by directly mixing cadmium carboxylate, elemental Se powder, and ODE at room temperature [17]. This featured a non-injection method for the synthesis of semiconductor nanocrystals in their quantum confinement size regime with high optical quality, and is referred to as the "non-injection approach" below. However, obtaining very small (with the first exciton absorption peak $\lesssim$520 nm) and very large (with the first exciton absorption peak $\gtrsim$620 nm) CdSe nanocrystals with the desired optical quality was found to be very difficult. This problem became apparent when these CdSe nanocrystals were used as the core nanocrystals for the growth of CdSe/CdS core/shell nanocrystals [23]. Because the non-injection nature dictates the nucleation temperature of the reaction (in the range 150–200 °C), it is difficult to balance the nucleation and growth needed to control the size and size distribution of the CdSe nanocrystals. Probably because of this problem, when this method was extended to the synthesis of other types of metal selenide nanocrystals, for example ZnSe nanocrystals (see the results below), the optical quality of the nanocrystals was found to be worse than those obtained using the standard injection method using Se–tributylphosphine as the Se precursor [24].

Several groups developed the Se–ODE solution approach in various forms by heating Se powder in ODE—without any metal ions or other reagents present—for a long period of time and at fairly high temperatures [18, 25–28]. A systematic study further suggested that the Se–ODE solution obtained by heating Se powder in ODE for 5 hours at 180 °C gave the best results [27]. In addition to the tedious heating process, using Se–ODE solutions as the Se precursor generally suffers from a relatively low reactivity in our hands (see later results). Dushkin's group reported loss of H_2Se gas on heating Se powder in ODE for an extended period of time [29], which suggests that the active Se species is converted into H_2Se gas probably in a similar manner as that observed on heating S in ODE [30]. Losing active Se species (as is confirmed below) not only may reduce the yield of the nanocrystals, but also can become a critical problem in certain circumstances. For instance, Mn doped ZnSe quantum dots (Mn:ZnSe d-dots) synthesized using a Se–ODE solution approach were found to be sensitive to most reagents, even ones as mild as oleic acid [31].

This report describes the use of stable suspensions

of fine Se powder in ODE (Se–SUS) as a high-performance, versatile, green, and convenient Se precursor for the synthesis of metal selenide nanocrystals. Se–SUS is simply made by shaking Se powder in ODE under ambient conditions. With CdSe and ZnSe as the basic model systems, this report focuses on a demonstration of the unique chemical features of Se–SUS, namely, high reactivity and excellent flexibility. Consequently, the unique advantages of Se–SUS will be exploited for achieving synthetic control of size/size distribution, volume yield, composition, optical properties, crystal structure, and alloying for a variety of high quality metal selenide nanocrystals, ranging from binary, core/shell, doped quantum dots (d-dots), and ternary metal selenides. Some of these are known synthetic challenges when using existing synthetic approaches available at present.

2 Results and discussion

2.1 Model system (CdSe and ZnSe core nanocrystals) study using Se–SUS

Syntheses of CdSe and ZnSe nanocrystals were used as the basic model systems for uncovering unique properties of Se–SUS.

Se–SUS was prepared by mixing Se powder (usually of 200 mesh) with ODE by 5 min sonication (or vigorous shaking by hand) under ambient conditions. Because ODE is quite viscous at room temperature, the suspension was found to be stable for several minutes. If visible separation of the Se powder from ODE was observed, a quick shake readily regenerated the uniform suspension. Syntheses using Se–SUS prepared in this manner were found to be reproducible, and reproducibility of the reactions with different sized Se powder, i.e., 100 and 200 mesh, was also excellent. This is likely because of the rapid melting/dissolution of the Se powder suspended in Se–SUS after being injected into the reaction solution at elevated temperatures. Consequently, some size variations of the Se powder should not be a main factor in determining the reproducibility of synthesis.

For the synthesis of CdSe (or ZnSe) nanocrystals, Cd (or Zn) fatty acid salts, a variable amount of free fatty acids, and ODE were heated together to form a clear solution. At a chosen reaction temperature, Se–SUS was injected into the reaction vessel to initiate the formation of CdSe (or ZnSe) nanocrystals. Details of typical syntheses for CdSe and ZnSe nanocrystals are provided in the Experimental section.

High quality CdSe and ZnSe nanocrystals in their quantum confinement size regime were synthesized using the Se–SUS approach (Fig. 1). X-ray powder diffraction revealed that the crystal structure of both CdSe and ZnSe nanocrystals had the zinc blende structure (Fig. S1 in the Electronic Supplementary Material (ESM)). The photoluminescence (PL) peak

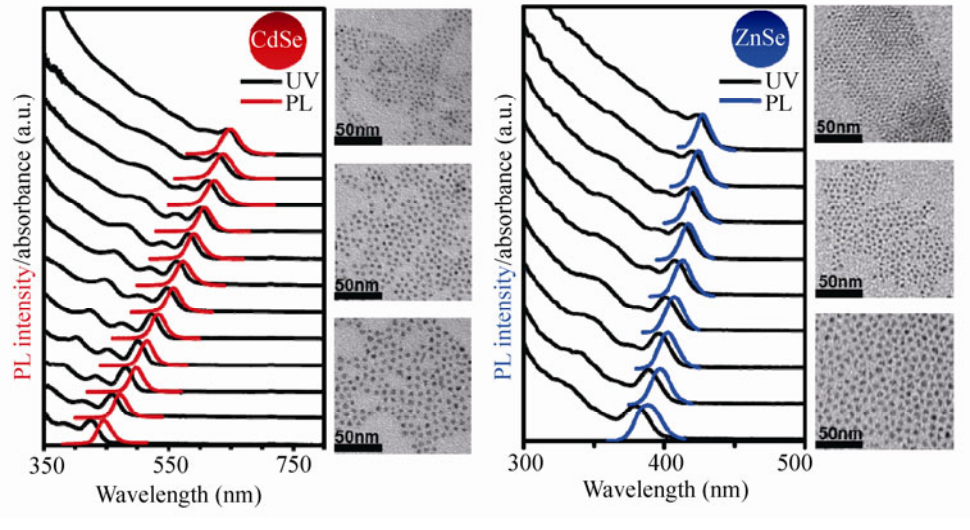

Figure 1 UV–vis, PL spectra and transmission electron microscopy (TEM) images of CdSe (left panel), ZnSe (right panel) nanocrystals with different sizes synthesized using the Se—SUS approach.

of the band edge emission of the resulting CdSe nanocrystals covered most of the visible window, i.e., approximately from 430 nm to 660 nm. The PL peak of the ZnSe nanocrystals ranged from 360 nm to 440 nm. For both systems, the PL full-width at half maximum height (FWHM) was found to be as narrow as ~85 meV. The sharp UV–vis absorption and PL spectra of these two types of binary metal selenide nanocrystals in the entire size regime are consistent with nearly monodisperse size distribution of the nanocrystals confirmed by TEM (Fig. 1).

2.2 Flexibility of Se–SUS and control of the size/size distribution as well as volume yield of nanocrystals

The final size and volume yield of both CdSe and ZnSe nanocrystals could be tuned by several different means, which demonstrates one aspect of the flexibility of Se–SUS. One method is to vary the initial injection temperature of Se–SUS. Generally speaking, a relatively low initial injection temperature results in a low nucleation temperature, and the nuclei concentration is relatively low. As a result, the final particle size is relatively large (Fig. S2, in the ESM). A second method is based on controlling the difference between the initial injection temperature and the subsequent growth temperature (Fig. S2, in the ESM). Preliminary results indicated that self-focusing [32] of size distribution—focusing of size distribution through ripening—played a key role in the growth of the nanocrystals in this approach. As a result, the final particle concentration was controlled by not only the initial injection temperature but also by the subsequent growth temperature. In addition, the nucleation–growth balance for size distribution control is also related to the temperature difference between the initial injection and subsequent growth.

A third method involves varying the concentration of either metal carboxylate or free fatty acid added to the reaction solution. Figure S3 in the ESM shows a spectral comparison of the stable nanocrystals for two reactions with identical conditions except for the concentration of either free fatty acids or metal carboxylates added.

The final method for varying the eventual size of the resulting metal selenide nanocrystals is through multiple injections of Se–SUS. This method can be employed for both controlling the final particle size and increasing the volume yield of the nanocrystals with a desired size. The latter feature is important for industrial production, given that semiconductor nanocrystals are actively being explored for commercial applications. For the synthesis of nanocrystals with large sizes, the initial injection can be optimized to grow nanocrystals with a relatively large size, and the subsequent secondary injections lead to further growth of the nanocrystals. Conversely, if the main purpose is to achieve a high yield of nanocrystals in one reaction (or high volume yield), the initial injection can be optimized to yield a large amount of nuclei and slow down the following self-focusing process by lowering the growth temperature. In both cases, in order to avoid occurrence of secondary nucleation, a relatively high concentration of either free fatty acids or metal carboxylates is necessary. A high acid concentration dissolves the tiny nuclei formed by secondary injections because the solubility of nanocrystals increases rapidly as their size decreases [33]. This effect can be readily detected by spectroscopy, especially PL (Fig. S4, in the ESM).

The four basic means discussed above were found to be effective for varying both the size and volume yield of the final products. In terms of the volume yield, there are several other points that need to be discussed. It was reported [27] and also confirmed by our own experiments that the solubility of Se in ODE is limited even upon prolonged heating. This sets a pretty low limit for the volume yield of metal selenide nanocrystals using Se–ODE solution approaches. Conversely, the amount of Se powder suspended in solution can be varied to include a much higher Se content. Preliminary results indicated that reactions performed with a Se–SUS precursor with ~10% (by mass) of Se in ODE could still yield CdSe nanocrystals with high optical quality. This is about 20 times higher than the maximum solubility of Se in ODE after 5 hours heating at 180 °C.

In comparison to the non-injection approach for the synthesis of CdSe nanocrystals, the volume yield of the process using Se–SUS can be increased significantly, especially for very small nanocrystals. Presumably, the synthesis of very small nanocrystals must be rapid and quenched almost immediately after the

initial formation of nuclei in a burst. Thus a high initial reaction temperature and immediate drop in the reaction temperature is a simple way to achieve a high volume yield of small nanocrystals. The Se–SUS approach presumably results in the formation of small nanocrystals at any temperature below the boiling point of the reaction mixture, roughly 300 ˚C. The initial reaction temperature for the non-injection approach, between 150 and 200 ˚C as mentioned above, is fixed by the initial melting/dissolution of the Se powder added to the reaction mixture at room temperature.

2.3 High reactivity and high conversion ratio of Se–SUS

As shown in Figs. 2(a) and 2(b), the conversions of elemental Se into either CdSe or ZnSe nanocrystals synthesized using Se–ODE solutions were only approximately 50%–60% of those for the corresponding reactions using Se–SUS. For a meaningful comparison, two reactions shown in Fig. 2(a) for the synthesis of CdSe nanocrystals (and Fig. 2(b) for the synthesis of ZnSe nanocrystals) were performed with identical molar amounts of Cd (or Zn), Se, and other reactants. Furthermore, the size of the resulting nanocrystals was adjusted to be the same. For the synthesis of CdSe nanocrystals as an example, the absorbance of the reaction solution at 320 nm—which is approximately

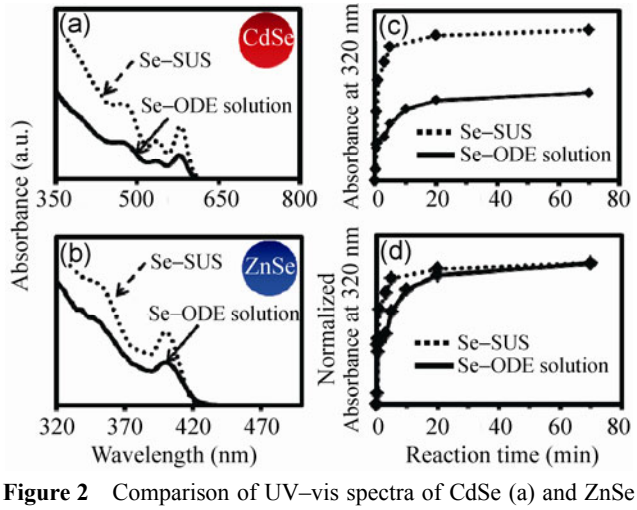

Figure 2 Comparison of UV–vis spectra of CdSe (a) and ZnSe (b) nanocrystals synthesized by Se–SUS and Se–ODE solution. (c) Absorbance at 320 nm of the reaction solution versus reaction time for the synthesis of CdSe nanocrystals. (d) The same results in (c) but normalized at a reaction time of 70 min.

independent of CdSe nanocrystal size [34] and thus can be used as a measure of CdSe unit yield in solution—for the reaction involving the Se–ODE solution was always significantly lower than that for the reaction involving Se–SUS (Fig. 2(c)). This clearly reveals that some of the Se was lost during the prolonged heating of Se powder in ODE at 180 ˚C, which is needed for dissolution of the Se powder in ODE to form the Se–ODE solution. Raston et al. demonstrated that the yield of CdSe nanocrystals using the Se–ODE solutions decreased as its heating time increased [27], which is in accordance with the results shown in Figs. 2(a) and 2(c).

Careful inspection of the solution absorbance at 320 nm for CdSe nanocrystals revealed that the missing part of Se in the Se–ODE solution is actually in the form of more reactive species. On normalizing the absorbance values at 70 min for both reactions in Fig. 2(c), the two normalized curves did not overlap (Fig. 2(d)). After normalization, the curve for the reaction associated with the Se–ODE solution is always below that for the Se–SUS case, except for the starting point and the normalization point. This means that the consumption of reactive Se species in the Se–ODE solution was significantly slower than that in the reaction performed with Se–SUS.

From the results in Figs. 2(c) and 2(d), it can be concluded that, in comparison with the Se–ODE solution, the Se–SUS not only contained 40%–50% more convertible Se specifies but also retained the more reactive Se species.

Experiments were designed to determine how the active Se species were lost during the preparation of the Se–ODE solution, in order to shed some light on the reaction pathways for Se–SUS. To mimic a typical synthetic reaction with Se–SUS, 2 mL Se–SUS (0.5 mol/L) was rapidly injected into a three-neck flask containing 5 mL of pure ODE at 300 ˚C. This reaction without any metal salts in place was stopped one hour after the injection. During the reaction, Ar was bubbled into the reaction solution and the gas phase mixture was led into a glass tube containing $Cd(NO_3)_2$ aqueous solution (Fig. 3).

Once the Se–SUS was injected into the flask loaded with hot ODE, the Se powder melted/dissolved rapidly and the solution became dark brown (Fig. 3(a)).

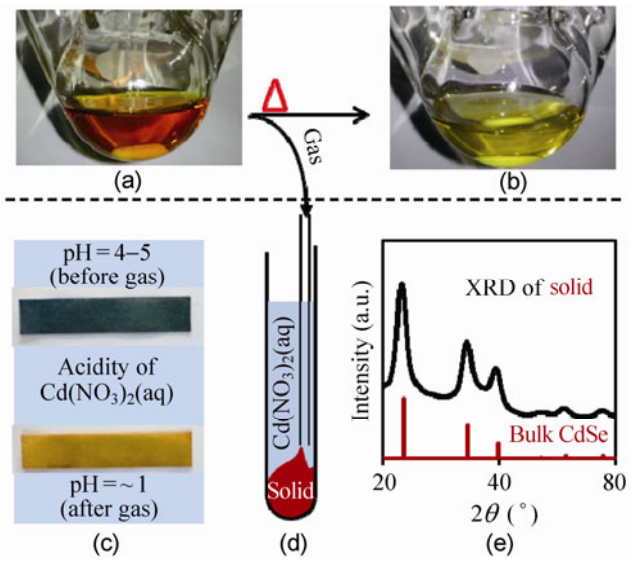

Figure 3 The color of the Se–ODE solution turned from dark brown (a) to bright yellow (b) after heating for an hour at 300 ˚C. (c) The pH test paper indicated that the pH of the $Cd(NO_3)_2$ aqueous solution turned from 4–5 (dark green) to 1 (yellow) after reacting with the gas. (e) XRD pattern of the red solid precipitated in the $Cd(NO_3)_2$ aqueous solution (d).

At the end of the reaction, the color of this solution turned bright yellow (Fig. 3(b)). At the same time, the $Cd(NO_3)_2$ solution in the glass tube reacted with the gas phase mixture from the solution and became turbid with some red precipitate at the bottom of the glass tube (schematically shown as Fig. 3(d)). The X-ray powder diffraction (XRD) pattern identified the red precipitate as CdSe (Fig. 3(e)). Quantitatively, the amount of Se found in the red precipitate in the glass tube accounted for ~50% of the total amount of Se powder injected into the reaction flask. This ratio is similar to the maximum ratio for the lost Se in Se–ODE solution reported by Dushkin's group [29]. Furthermore, along with formation of the red CdSe precipitate, pH measurements of the $Cd(NO_3)_2$ aqueous solution indicated formation of acidic species in the aqueous solution (pH 4–5 before reacting with the gas and pH ~1 after the reaction, Fig. 3(c)). All of this evidence is consistent with the generation of H_2Se by the reaction of Se powder and ODE in the reaction flask.

In summary, Se powder and ODE can react to form an active Se species at elevated temperatures. During preparation of the Se–ODE solution, since the reaction solution does not contain any metal ions, the active Se species react further with ODE to form H_2Se. As H_2Se is a highly volatile species at the temperatures used for preparing the Se–ODE solution, it evaporates into the gas phase. After heating a mixture of Se powder and ODE for a long time, all the active Se species are consumed and only the less active Se species—not volatile at the preparation temperature of the Se–ODE solution—are retained in the Se–ODE solution. If there are any metal salts (such as Cd and Zn fatty acid salts) in the solution, the active Se species will react with the metal ions to form metal selenides. As a result, the synthesis of metal selenide nanocrystals using the Se–SUS approach should be both fast and high yield in comparison to the corresponding reactions using the Se–ODE solution approach (Fig. 2).

It should be pointed out that the exact reaction pathway in the formation of either CdSe or ZnSe nanocrystals is largely unknown at this moment. Although formation of H_2Se during the preparation of Se–ODE solutions is strongly supported by the results shown in Fig. 3, it is impossible at present to determine if H_2Se played a role in the formation of CdSe and ZnSe nanocrystals. To fully clarify the reaction mechanism, a systematic and careful study is needed.

The highly reactive nature of Se–SUS is important not only for increasing the volume yield of nanocrystals shown in Fig. 2, but also in the control of the quality of the resulting nanocrystals. This will be demonstrated in several cases below. For ZnSe nanocrystals synthesis, Se–SUS made the synthesis of high quality ZnSe nanocrystals even easier than that using highly toxic Se–tributylphosphine. When Se–tributylphosphine was used as the Se precursor and zinc fatty acid salts as the Zn precursor in ODE, formation of high quality ZnSe nanocrystals was only feasible if a certain amount of fatty amines were added as the activation reagent and the reaction temperature was as high as 330 ˚C [24]. Without fatty amines added, the concentration of ZnSe nanocrystals formed in a typical Se–organophosphine approach was extremely low and the size distribution was hard to control. Evidently, when Se–SUS was employed in this work, formation of high quality ZnSe nanocrystals with high yield could be achieved without addition of

amine (see "Synthesis of 4 nm ZnSe nanocrystals using Se–SUS" in the Experimental section as an example). In addition, the high reactivity of Se–SUS enabled significantly lower reaction temperatures (~240–290 ℃), instead of the relatively high reaction temperatures (~310–360 ℃) required in the case of Se–tributylphosphine being used as the Se precursor.

It should be pointed out that, although grown at a relatively low temperature, the ZnSe nanocrystals from the Se–SUS approach were found to be of high quality. For instance, the comparative advantages of the Se–SUS approach over the non-injection approach—mixing Se powder, zinc fatty acid salts, and ODE at room temperature and heating the mixture together—were found to be substantial. As shown in Fig. 4, the absorption and PL spectra of the ZnSe nanocrystals synthesized using the Se–SUS approach were significantly sharper than those synthesized with the non-injection approach. Furthermore, the relative PL quantum yield (QY)—defined as the PL intensity divided by the absorbance at the excitation wavelength—of the ZnSe nanocrystals from the Se–SUS approach was about 10 times higher than that of the nanocrystals from the non-injection approach. As will be described below, these optical quality features of the ZnSe nanocrystals were found to be inherited by ZnSe/ZnS core/shell nanocrystals.

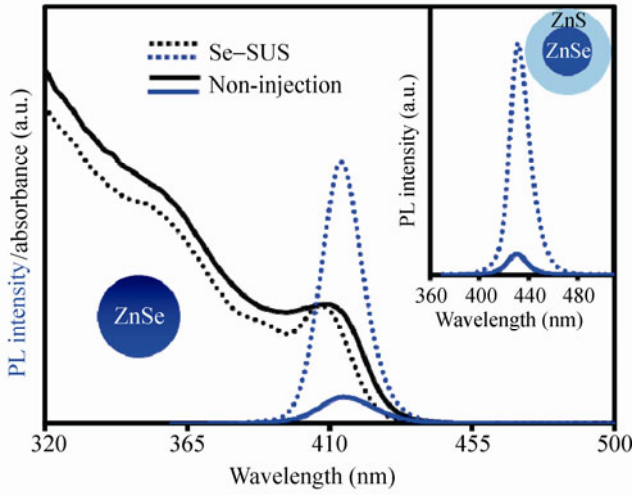

Figure 4 UV–vis and PL spectra of ZnSe nanocrystals synthesized by Se–SUS and non-injection approach. Inset: PL of ZnSe/ZnS core/shell nanocrystals with the same shelling scheme but with different synthetic methods for the cores, Se–SUS (⋯) and non-injection (—).

2.4 ZnSe and CdSe core nanocrystals synthesized using the Se–SUS approach for core/shell growth

While core nanocrystals were synthesized with high quality, this does not guarantee that the subsequent epitaxial growth of the shell materials will be successful. This is so because the subsequent epitaxial growth requires the surface structure and ligand chemistry of the core nanocrystals to be compatible with the precursors/conditions for the shell growth. For instance, the growth of CdSe based core/shell nanocrystals with the zinc blende structure remained a challenge until very recently [23], although high quality CdSe core nanocrystals with the zinc blende structure were reported in 2005 [35]. Experimental studies of epitaxial growth with various shelling materials, including ZnS, ZnSe, and CdS, all indicate that the zinc blende core nanocrystals formed via the Se–SUS approach were suitable for formation of high quality core/shell nanocrystals.

The source of the ZnSe core nanocrystals was found to play a critical role in the growth of high quality ZnSe/ZnS core/shell nanocrystals. When using two different types of ZnSe core nanocrystals (shown in Fig. 4) for the epitaxial growth of ZnSe/ZnS core/shell nanocrystals, the resulting ZnSe/ZnS core/shell nanocrystals showed substantial difference in optical quality. The ZnSe nanocrystals synthesized through the Se–SUS approach yielded ZnSe/ZnS core/shell nanocrystals with PL QY in the range between 40%–60%. This value is ten times that of the PL QY for the core/shell nanocrystals grown with the core nanocrystals from the non-injection approach (Fig. 4 inset). Furthermore, these ZnSe/ZnS core/shell nanocrystals could be potential candidates as Cd-free UV–blue emitting nanocrystals to replace the CdS/ZnS ones reported previously [36].

The two types of ZnSe/ZnS core/shell nanocrystals shown in Fig. 4 (inset) further showed significant difference in PL peak width, i.e., about 23% narrower for the ones with the core nanocrystals from the Se–SUS approach. Because the shelling procedure and conditions were identical for the two experiments shown in Fig. 4 (inset), one might suspect that the difference in optical properties, both PL QY and PL peak width, is a result of a difference in the quality of the core nanocrystals illustrated in Fig. 4.

Figure 5(a) illustrates the evolution of the UV–vis and PL spectra of ZnSe—synthesized using the Se–SUS approach—and ZnSe/ZnS core/shell nanocrystals during the growth of about five monolayers of ZnS shell. The UV–vis and PL spectra revealed a gradual red shift as expected for epitaxial growth instead of alloying. The relative PL quantum yield increased significantly as the shell thickness increased and reached a plateau (Fig. 5(b), blue curve). At the same time, shelling initially decreased the PL FWHM and then increased it somewhat (Fig. 5(b), black curve). Such a trend in PL band width change, to our knowledge, was only reported recently for the successful epitaxial growth of CdSe/CdS core/shell nanocrystals with the zinc blende structure [23], and was considered to be the result of nearly perfect surface passivation by epitaxial growth of the shell semiconductor material.

The XRD patterns of both ZnSe core and ZnSe/ZnS core/shell nanocrystals (Fig. 5(c)) were found to be characteristic of the zinc blende structure. With five monolayers of ZnS on the surface of a 5.0 nm ZnSe core nanocrystal, the diffraction peaks of the core/shell nanocrystals shifted to those of pure ZnS nanocrystals due to the dominating volume fraction of the ZnS component in the core/shell nanocrystals. These results again are consistent with successful epitaxial growth of ZnS layers with the zinc blende structure onto the core nanocrystals. The TEM results shown in Fig. 5(d) reveal the expected particle size increase due to the shell growth. The size distribution of the core/shell nanocrystals almost retained that of the core nanocrystals.

Recent reports have indicated that the use of CdSe core nanocrystals with relatively small sizes (with their PL peak <540 nm) often resulted in CdSe/CdS core/shell nanocrystals with distorted and broad PL spectra [23]. Our results revealed that the CdSe nanocrystals with small sizes synthesized using the Se–SUS approach yielded CdSe/CdS core/shell nanocrystals with significantly narrower and more symmetric PL spectra (Fig. S5 in the ESM). Furthermore, using CdSe nanocrystals with medium sizes (with their PL peak in the range 540–580 nm) from the Se–SUS approach effectively eliminated a small PL peak on the high energy side of the main PL peak observed for the CdSe/CdS core/shell nanocrystals (Fig. S5 in the ESM).

We believe the problematic PL features reported in Ref. [23] and shown in Fig. S5 in the ESM resulted from the nature of the core nanocrystals synthesized using the non-injection approach. CdSe nanocrystals

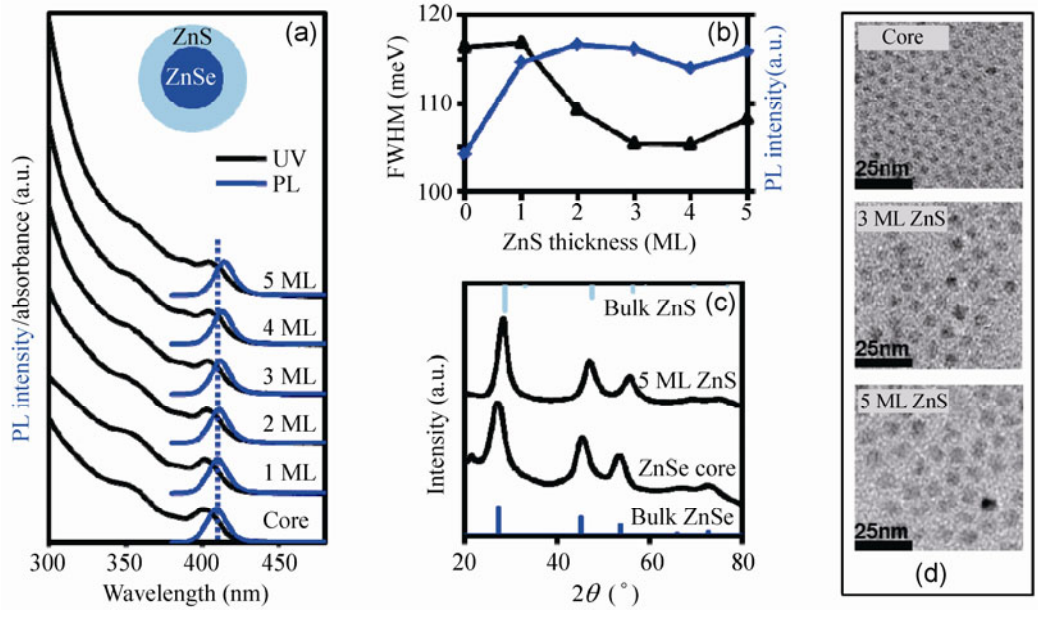

Figure 5 (a) UV–vis and PL spectra of ZnSe/ZnS core/shell nanocrystals with different shell thicknesses. (b) Evolution of relative PL QY and FWHM during growth of the ZnS shell. (c) XRD patterns of ZnSe core and ZnSe/ZnS core/shell nanocrystals with five monolayers (5 ML) of ZnS. (d) TEM images of ZnSe nanocrystals with 0, 3, and 5 ML of ZnS. The size of the ZnSe core nanocrystals was 5 nm.

with small and medium sizes need relatively low reaction temperature and short reaction time. Consequently, there could be some very small nanocrystals in the sample, which are not easily detected by either UV–vis or PL spectroscopy. Upon the growth of CdS shells onto these tiny CdSe nanocrystals in the core sample, the resulting small core/shell nanocrystals with tiny cores became as efficiently emissive as the large ones in the same sample, and can thus be detectable by the PL measurements. This makes the PL spectrum broad and asymmetric by creating a tail (or a secondary peak) on the high energy side of the PL peak for the core/shell nanocrystals (Fig. S5, in the ESM).

2.5 Se–SUS as the Se precursor for shell growth

At present, the most common shell materials for the synthesis of core/shell nanocrystals are metal sulfides and metal selenides. For the epitaxial growth of metal sulfides, diethyldithiocarbamate and elemental sulfur dissolved in ODE have been proven to be green, widely applicable, yet high-performance, S precursors. To our knowledge, the most commonly used Se shelling precursors are still Se–organophosphine and bis-trimethylsilyl selenide [37–39], which are toxic, expensive, and not easy to handle.

Figure 6 illustrates the process of epitaxial growth of a ZnSe shell onto CdSe core nanocrystals synthesized using the Se–SUS approach. For the epitaxial growth of the shell, zinc fatty acid salts and Se–SUS along with a certain amount of fatty amine were added at a relatively low temperature to avoid self-nucleation of the shell materials, and then, temperature was increased to the reaction temperature for the growth of one monolayer of ZnSe. This process is known as thermal cycling [40].

TEM measurements confirmed that the average size of the CdSe/ZnSe core/shell nanocrystals was consistent with the expected increase in the shell growth, whilst the size distribution of the core/shell nanocrystals remained similar to that of the original core nanocrystals (Fig. 6(a) and Fig. S6 in the ESM). Figure 6(b) shows that both UV–vis and PL spectra of the core/shell nanocrystals were red-shifted significantly upon the growth of the ZnSe shell onto the CdSe core nanocrystals. Furthermore, the relative PL QY of the CdSe/ZnSe core/shell nanocrystals was

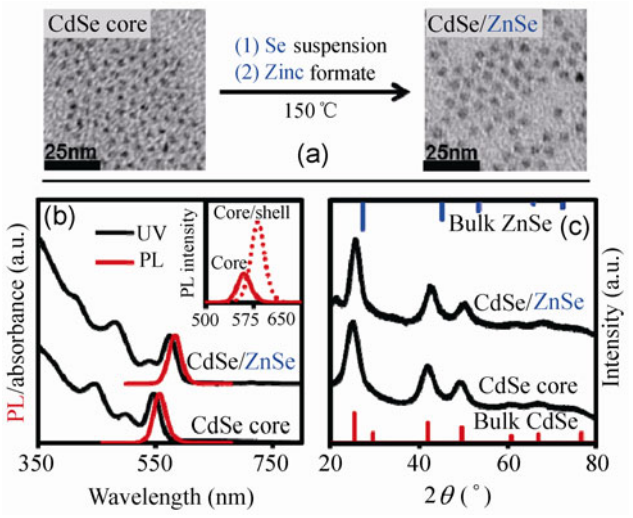

Figure 6 TEM (a), UV–vis and PL spectra (b), XRD pattern (c) of CdSe core and CdSe/ZnSe core/shell nanocrystals. The inset in (b) shows the PL intensity of the CdSe core (—) and CdSe/ZnSe core/shell (⋯) nanocrystals.

found to increase significantly after shell growth (Fig. 6(b) inset). These results are consistent with a homogeneous shell growth, instead of significant alloying. Consistent with epitaxial growth, the crystal structure of both core and core/shell nanocrystals was determined to be zinc blende (Fig. 6(c)).

For CdSe/ZnSe core/shell nanocrystals, alloying was found to be dependent on the growth temperature of the ZnSe shell. The results shown below will demonstrate that Se–SUS is an excellent Se precursor for lowering the shelling temperature because of its highly reactive chemical nature (see Fig. 2(d) and the related text). Thus, it was possible to tune the shelling temperature by adjusting the reactivity of the zinc precursor, i.e., zinc carboxylates.

When zinc stearate (or zinc oleate) was employed as the zinc precursor, the temperature required for the epitaxial growth of the ZnSe shell was about 250 ℃. It has been reported that Cd and Zn can undergo alloying even at a temperature as low as 200 ℃ [41]. This was confirmed in the current system by observing significant blue-shifts of PL peaks during the ZnSe shell growth using zinc stearate as the Zn precursor (Fig. S7 in the ESM). By shortening the chain length of the fatty acid salts used, the shelling temperature was reduced to 210 ℃ for zinc acetate. This temperature was further reduced to 150 ℃ for zinc formate

and this relatively low reaction temperature prevented alloying during the shell growth.

2.6 Synthesis of high quality Mn:ZnSe d-dots using Se–SUS

Transition metal doped quantum dots are currently being explored as both emissive materials and spintronic materials [4–7]. Because optical emission of d-dots is associated with d orbitals and its photon energy is significantly smaller than the bandgap, d-dots possess a substantial Stokes shift. This feature becomes important when high concentrations of emitters are necessary, such as in light emitting diodes and solid state lighting devices. Atomic d orbitals as the emission energy levels also enable high thermal stability of the emission [42]. Chemical stability of d-dots was reported to be excellent as long as the emissive dopant ions were located away from the surface [43]. If the host materials and dopant ions are carefully chosen, such as Mn:ZnSe d-dots, the emitters can be Cd-free. At present, the most common host for d-dots as Cd-free emissive nanocrystals is ZnSe, which yields d-dots with high PL QY (>50%) [42].

The original ZnSe based d-dots with high PL QY were grown with Se–organophosphine as the Se precursor [5]. In addition to the problems of toxicity and pyrophoric nature of organophosphines, the Se–organophosphine seemed to be not sufficiently reactive. For example, up to a 50-fold excess of Se–tributylphosphine was needed for a reasonable synthesis of MnSe seeds [42]. Furthermore, Mn:ZnSe d-dots with acceptable chemical/thermal stability were only successfully synthesized by the use of pre-synthesized MnSe nanoclusters as the seeds followed by the over-coating of ZnSe host material, a process which is known as "nucleation doping". In this manner, the Se–organophosphine precursor present in a huge excess was forced to react with Mn carboxylate in the absence of any Zn ions. Numerous attempts at "co-nucleation doping" with both Mn carboxylate and Zn carboxylate in the initial reaction solution all failed to reach the same optical quality, at least in our group.

Recently, Se–ODE solution in various forms was explored for the growth of ZnSe based d-dots to eliminate the environmental and safety concerns of organophosphines [25, 28]. However, our results revealed that the Se–ODE solution seemed to be even less reactive than the Se–organophosphine as the Se precursor. As a result, synthesis of Mn:ZnSe d-dots using the Se–ODE solution required a long reaction time at elevated temperatures [44]. At the optimized temperature, i.e., 240 ℃, the over-coating of ZnSe host material took more than one hour to reach the desired PL QY of ~50%. This lengthy process is not only time consuming but also results in chemically unstable d-dots that could not even withstand mild chemical reagents, such as oleic acid [31]. Detailed structural analysis revealed that the dopant ions in the Mn:ZnSe d-dots synthesized using the Se–ODE solution were widely spread throughout the entire nanocrystal including the surface [31]. This structural feature was likely caused by the activation of Mn ion diffusion in the nanocrystals by the lengthy heating process at elevated temperatures [44], and is probably responsible for the high sensitivity to common reagents.

The use of active Se–SUS precursor enabled co-nucleation doping affording high quality Mn:ZnSe d-dots (Fig. 7). UV and PL spectra of the d-dots are shown in Fig. 7(a). No bandgap emission of undoped ZnSe nanocrystals was observed. The typical PL QY of the Mn:ZnSe d-dots synthesized using this new method was reproducibly above 50%, which is at least comparable to the values reported for the d-dots formed by the nucleation-doping with pre-synthesized MnSe nanoclusters using the Se–organophosphine precursors. Suppressed bandgap emission of pure ZnSe and high PL QY of d-dots imply that the resulting d-dots formed through this doping strategy were of high purity, i.e., almost no undoped ZnSe nanocrystals were formed in the synthesis.

A potential application of d-dots is as the down conversion emissive materials for solid state lighting, given their large Stokes shift (Fig. 7(a)) and outstanding thermal stability. The current mainstream excitation wavelength from GaN light emitting diodes (LEDs) lies around 450 nm. The UV–vis spectrum of the d-dots shown in Fig. 7(a) indeed possessed a reasonable absorption at 450 nm, which is very close to the absorption properties of a bulk sample. TEM measurements in Fig. 7(b) (inset) confirmed the d-dots had a

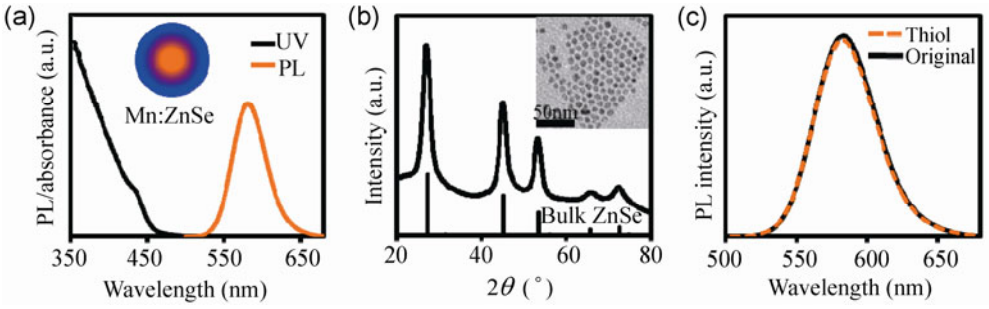

Figure 7 (a) UV–vis and PL spectra of the Mn:ZnSe d-dots formed by co-nucleation doping using Se–SUS as the Se precursor. (b) XRD pattern and TEM image (inset) of the Mn:ZnSe d-dots. (c) PL spectra of the Mn:ZnSe d-dots before (dark line) and after (orange line) thiol exchange.

very large size, ~10 nm. The TEM results further revealed a nearly monodisperse size distribution of these large nanocrystals. The XRD pattern (Fig. 7(b)) indicates that the d-dots have the zinc blende structure with quite sharp diffraction peaks. All these results indicate that the highly reactive Se–SUS precursor enabled rapid growth of the ZnSe host material—only about 30 min was required for the growth of the d-dots shown in Fig. 7—and offered excellent control of the optical as well as structural properties of the d-dots.

The thermal stability of the d-dots synthesized using the Se–SUS approach was comparable to that of those synthesized through the conventional Se–organophosphine approach [42] (Fig. S8 in the ESM). To measure the chemical stability, a well-known [43] quencher—an aliphatic thiol—was employed. The results in Fig. 7(c) reveal that no noticeable PL quenching was observed on addition of thiols to the purified d-dots solution. In fact, d-dots synthesized using the Se–SUS approach were found to be stable against all types of common reagents tested, including fatty acid, amines, thiols, and common solvents.

The highly active nature of Se–SUS demonstrated above shows that this new approach not only eliminates the need for toxic and pyrophoric organophosphines in the synthesis of d-dots, but also offers the necessary flexibility for further development of the synthetic chemistry for this type of complex nanocrystals. For instance, preliminary results indicate that this new approach could yield d-dots with simpler and more controlled PL decay dynamics than that observed using the d-dots grown by the conventional Se–organophosphine approach. The details of such studies will be the subject of a separate publication.

2.7 Synthesis of complex composition nanocrystals using Se–SUS as the Se precursor

Ternary, tertiary, and other types of intrinsic semiconductor nanocrystals with complex compositions are gradually moving into the center of the field of semiconductor nanocrystals [45–48]. At present, the most widely explored nanocrystals with complex composition are metal sulfides and metal selenides. Complexity in composition presumably adds one parameter for controlling the intrinsic semiconductor properties, such as band gap, band alignments, absorption coefficients, and conductivity. Unfortunately, complexity in composition dramatically complicates the synthetic chemistry of the corresponding nanocrystals [45–48]. One of key issues which has been identified is how to balance the reactivity of multiple cations/anions in the reaction solution to avoid inhomogeneity of composition in a nanocrystal. Here, Se–SUS will be explored as the Se precursor to tackle this problem using $CuInSe_2$ and $CuInSe_2$/ZnSe core/shell nanocrystals as an example.

The direct band gap of bulk $CuInSe_2$ is 1.0 eV, which makes it well suited for use as a solar cell material and a light emitting material. When Se–SUS was employed as the Se precursor, formation of $CuInSe_2$ nanocrystals occurred in a temperature range as low as between 100 and 180 °C. Because the reactivities of Cu and In ions towards chalcogenides are dramatically different [45], the relatively low reaction temperature offered by an reactive Se precursor seems to be quite

helpful. This is particularly true for the very small $CuInSe_2$ nanocrystals that are needed for the development of emissive nanocrystals in the visible optical window, provided by the relatively narrow bulk band gap of $CuInSe_2$.

As shown in Fig. 8(a), the optical absorption edge of the $CuInSe_2$ nanocrystals synthesized using Se–SUS as the Se precursor could be tuned in a large wavelength window. Most of these nanocrystals were too small to be measured reliably using TEM, i.e., the size range is smaller than 2 nm. Moreover, similar to other types of semiconductor nanocrystals with very small sizes, the PL of the $CuInSe_2$ nanocrystals shown in Fig. 7(a) was either very weak or not measureable. Using Se–SUS and zinc fatty acid salts, these $CuInSe_2$ nanocrystals were coated with ZnSe shell to form $CuInSe_2$/ZnSe core/shell nanocrystals. The PL of $CuInSe_2$/ZnSe core/shell nanocrystals was greatly enhanced after the growth of the ZnSe shell and tunable emitters with reasonable PL QY were obtained in the color range covering yellow, orange, red, and near infrared (Fig. 8(b)). Without optimization, the PL QY of the $CuInSe_2$/ZnSe core/shell nanocrystals was determined to be up to ~35%.

The $CuInSe_2$/ZnSe core/shell nanocrystals were found to be a zinc blende phase (Fig. 8(c)), which should not lead to problems as far as emissive materials are concerned. However, the literature indicates that the ordered chalcopyrite phase of $CuInSe_2$ is of most interest for photovoltaic applications [49]. One potential route towards high performance solar cells is to fabricate thin films using $CuInSe_2$ nanocrystals. To reduce the electronic defects in the thin films, ordered chalcopyrite phases of $CuInSe_2$ nanocrystals with large grain sizes are desirable. Using the Se–SUS precursor, we synthesized the chalcopyrite phase of $CuInSe_2$ at 180 ˚C. The XRD pattern (Fig. 8(d)) confirmed the correct crystal structure, and the average grain size was estimated to be around 1,100 nm from the peak width in the XRD pattern using Scherrer's equation. Based on preliminary results, the crystal structure control (comparing the patterns in Figs. 3(c) and 3(d)) achieved here seems to be a result of the reaction rate: High reaction rate yielded chalcopyrite microcrystals and a relatively slow rate generated the zinc blende nanocrystals.

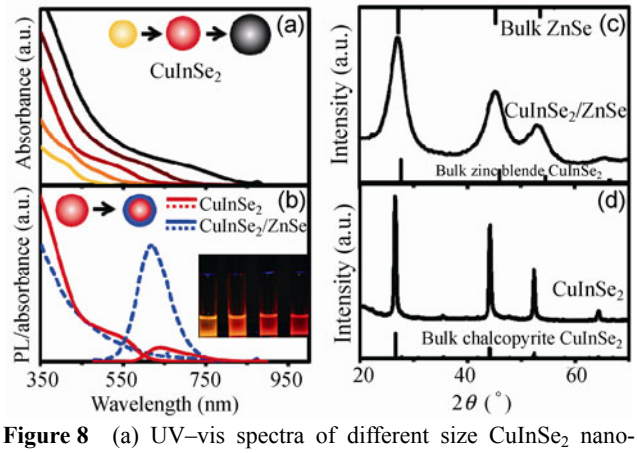

Figure 8 (a) UV–vis spectra of different size $CuInSe_2$ nanocrystals. (b) UV–vis and PL spectra of $CuInSe_2$ nanocrystals before and after coating with ZnSe. (c) XRD pattern of the chalcopyrite phase of $CuInSe_2$ nanocrystals. (d) XRD pattern of $CuInSe_2$/ZnSe core/shell nanocrystals.

2.8 Purification/isolation of the nanocrystals made by the Se–SUS approach

Purification here refers to the removal of unused starting materials and side products with the nanocrystals still in solution form, and isolation means obtaining a powdery form of the nanocrystals only with their surface ligands. In many cases, colloidal nanocrystals are directly employed in solution, and thus the presence of solvents and certain other molecules in the solution is not a concern. For instance, for epitaxial growth of shell materials, complete isolation without any solvent was found not only to be unnecessary but also to cause problems such as aggregation, for which an *in situ* purification procedure reported recently [23] worked well. Below, an isolation procedure (Fig. 9) will be discussed using CdSe nanocrystals as an example.

The isolation procedure involves two extraction steps using an ODE/hexane–ethanol bi-phase system. Butylamine was added in the first extraction step to enhance the removal of fatty acids and carboxylate salts into the ethanol phase, and chloroform was added in the precipitation step to retain the non-polar yet non-volatile liquid, i.e., ODE, in the polar acetone phase. The FTIR spectra in Fig. 9(b) reveal that one extraction step removed approximately 70% of metal carboxylates, which are difficult to eliminate by simple precipitation. After the extraction and precipitation,

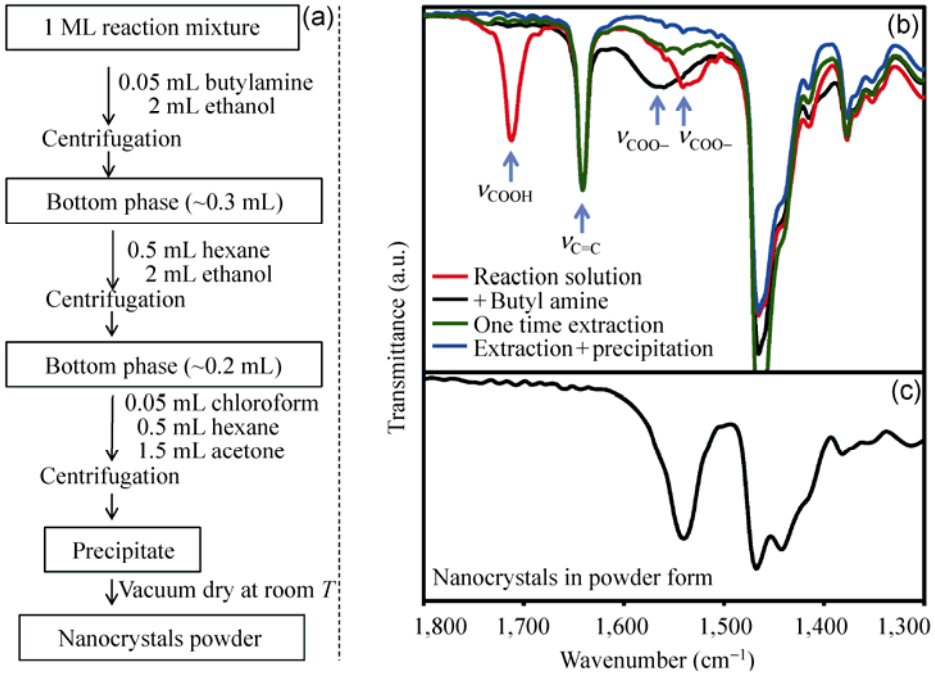

Figure 9 (a) Isolation procedure for CdSe nanocrystals synthesized using the Se–SUS approach. (b) FTIR spectra of nanocrystal solutions at different stages using the C=C double bond of ODE as an internal reference. (c) FTIR spectrum of the final product, i.e., nanocrystals coated with ligands in powder form.

the FTIR spectra in Fig. 9(b) indicate that nearly all the free fatty acids and carboxylate salts were removed. The FTIR spectrum of the final product after drying in vacuum (Fig. 9(c)) illustrates that ODE was not detectable and only carboxylate surface ligands were observed.

In each extraction step and subsequent precipitation step, the upper phase was always colorless. This means that the nanocrystals were retained in either the ODE/hexane phase in the extraction or the precipitate in the precipitation step, which ensured a nearly quantitative recovery of the nanocrystals. Centrifugation was employed for both extraction and precipitation steps to shorten the separation times. Similar to the *in situ* purification procedure [23], the isolation procedure described in Fig. (9) employs extraction, which helps to maintain good colloidal dispersibility of the final products in comparison with a procedure with multiple precipitation steps.

2.9 Comparison of Se–SUS with other approaches using Se powder

There are two classes of synthetic approaches using Se powder. The first one is the non-injection approach [17]. Compared with this non-injection approach, the Se–SUS approach possesses valuable flexibility in terms of tuning the nucleation temperature, amount of Se element in a reaction, single/multiple injections, and the sequence of injections for the synthesis of d-dots and core/shell dots. In addition, such flexibility also enables tunability of the reactivity of the Se precursor, which is the other main chemical feature of the Se–SUS approach. Lacking these two features, the non-injection approach is not be applicable for solving several synthetic challenges described above, such as synthesis of core/shell nanocrystals, d-dots, and tertiary nanocrystals. In principle, any reaction requiring hot injections, especially multiple injections, is challenging for the non-injection approach based on Se powder.

The representative example of the second class of synthetic approaches is the one based on Se–ODE solutions. As shown in Figs. 2 and 3, the prolonged heating required to dissolve Se powder in ODE removes highly reactive Se species. As a result, the Se–ODE solutions cannot fulfill some of the accomplishments

of the Se–SUS approach, such as the synthesis of chemically stable d-dots, development of co-nucleation for d-dots, and prevention of alloying in core/shell growth.

Cao's group reported a non-injection synthesis for CdSe nanocrystals using SeO_2 powder [19]. Under similar reaction conditions, the initial reaction temperature required for the formation of CdSe nanocrystals in the non-injection synthesis using SeO_2 powder (~240 ℃) was found to be significantly higher that required when using Se powder (~200 ℃) [19]. This implies that the tunability of the reactivity of SeO_2 powder is limited in comparison with that of Se powder. Furthermore, the relatively high reaction temperature required for the SeO_2 powder means that it is not suitable for application in several synthesis demonstrated above, such as epitaxial growth of ZnSe shells onto CdSe nanocrystals. In addition, our preliminary results indicated that SeO_2 powder could not be stably dispersed as a suspension in ODE for realization of hot injections.

3 Experimental

3.1 Chemicals

Tetramethylammonium hydroxide (98%), zinc stearate ($ZnSt_2$, ZnO (12.5%–14%)), Se (200 and 100 mesh, 99.999%), ODE (90%), cadmium oxide CdO (99.998%), cadmium acetate dihydrate ($CdAc_2{\cdot}2H_2O$, 98.5%), stearic acid (HSt, 90 +%), zinc acetate dihydrate ($ZnAc_2{\cdot}2H_2O$, 99.99%), sodium diethyldithiocarbamate trihydrate (NaDDTC· $3H_2O$, 99%), zinc formate (98%), octylamine (98%), manganese chloride ($MnCl_2$, 99%), 1-dodecanethiol (98%), indium acetate ($InAc_3$, 99.99%), oleic acid (90%), and butylamine (98%) were purchased from Alfa- Aesar. Oleylamine (90%) was purchased from Acros. Tributylphosphine was purchased from Shanghai Titan Chem. Copper(I) acetate (CuAc, 99.999%) was purchased from TCI. All organic solvents were purchased from Sinopharm Reagents.

3.2 Synthesis of $CdSt_2$

In a typical synthesis, $CdAc_2$ (10 mmol) was dissolved in methanol (20 mL) in a 50 mL flask. In a separate 500 mL flask, HSt (20 mmol) and tetramethylammonium hydroxide (20 mmol) were dissolved in methanol (100 mL) by stirring for 20 min. To this solution, the $CdAc_2$ solution was added dropwise with vigorous stirring; white precipitation indicated the formation of $CdSt_2$. After addition of the $CdAc_2$ solution, stirring was continued for 20 min. The precipitate was washed three times with methanol, and dried under vacuum overnight before using.

3.3 Synthesis of $MnSt_2$

The procedure was similar to the synthesis of $CdSt_2$, except for substitution of $MnCl_2$ for $CdAc_2{\cdot}2H_2O$.

3.4 Synthesis of $Zn(DDTC)_2$

In a typical synthesis, NaDDTC (20 mmol) was dissolved in distilled water (60 mL). In a separate flask, $ZnAc_2{\cdot}2H_2O$ (10 mmol) was dissolved in distilled water (40 mL). To this solution, the NaDDTC solution was added dropwise with vigorous stirring; white precipitation indicated the formation of Zinc diethyldithiocarbamate trihydrate ($Zn(DDTC)_2$). After addition of the NaDDTC solution, stirring was continued for 20 min. The precipitate was washed three times with distilled water, and dried under vacuum overnight before using.

3.5 Synthesis of 2.2 nm CdSe nanocrystals using Se–SUS

In a typical synthesis, $CdSt_2$ (0.0678 g, 0.1 mmol) was loaded into a 25 mL three-neck flask with 4 mL of ODE. After stirring and argon bubbling for 10 min, the mixture was heated to 250 ℃. The Se–SUS was prepared by dispersing Se powder (0.0118 g, 0.15 mmol) in ODE (3 mL) by sonication for 5 min. 1 mL of the Se–SUS was injected quickly into the reaction flask at 250 ℃ and the reaction temperature was decreased to 220 ℃ by the injection. The reaction temperature was set to 220 ℃ for further growth of the nanocrystals. Needle-tip aliquots were taken and dissolved in toluene for UV–vis and PL measurements to monitor the reaction.

3.6 Synthesis of 3.0 nm CdSe nanocrystals using Se–SUS

In a typical synthesis, $CdSt_2$ (0.0256 g, 0.2 mmol) and

HSt (0.2845 g, 1 mmol) were loaded into a 25 mL three-neck flask with 4 mL of ODE. After stirring and argon bubbling for 10 min, the mixture was heated to 240 ˚C. 1 mL of the 0.1 M Se–SUS (see above for preparation) was injected quickly into the reaction flask at 240 ˚C. The reaction temperature was kept at 240 ˚C for further growth. Needle-tip aliquots were taken and dissolved in toluene for UV–vis and PL measurements to monitor the reaction.

3.7 Multiple injection synthesis of 4.5 nm CdSe nanocrystals

In a typical synthesis, CdO (0.0256 g, 0.2 mmol) and HSt (0.2845 g, 1 mmol) were loaded into a 25 mL three-neck flask with 4 mL of ODE. After stirring and argon bubbling for 10 min, the mixture was heated to 250 ˚C. 0.1 M Se–SUS (0.5 mL, prepared above) was injected quickly into the reaction flask at 250 ˚C. The reaction temperature was kept at 250 ˚C for further growth. After growth for 10 min, another shot of 0.1 M Se–SUS (0.1 mL) was injected into the reaction solution. About 3–4 min later, the third injection (0.05 mL of Se–SUS) was added. Multiple injections were repeated every 3–4 min with the amount for each injection being 0.03 mL of Se–SUS until the size of the nanocrystals reached 4.5 nm. Needle-tip aliquots were taken and dissolved in toluene for UV–vis and PL measurements to monitor the reaction.

3.8 Isolation of CdSe nanocrystals

The isolation process is briefly illustrated in Fig. 9(a) and was found to be applicable to all nanocrystals described here. In a typical purification, reaction solution (1 mL) was added to a 4 mL glass vial. Into the vial, 0.5 mL of butylamine and 2 mL of ethanol were added for the first extraction. The mixture was maintained at 50 ˚C for 5 min. After shaking and centrifugation, the upper ethanol phase was removed. For the second extraction, hexane (0.5 mL) and 2 mL of ethanol were added. In the same way, the upper ethanol phase was removed after centrifugation. Chloroform (0.05 mL), 0.5 mL of hexane, and 1.5 mL of acetone were added sequentially. After centrifugation, the precipitate of nanocrystals was collected by decantation of the supernatant. For the synthesis of CdSe nanocrystals (~2.8 nm in size, with first excitonic absorption peak at 542 nm) using 0.2 mmol of cadmium stearate and 0.1 mmol of Se powder, the mass of the final CdSe nanocrystals product after vacuum drying at room temperature was 0.045 g. Assuming a full monolayer of stearate ligands (bound onto excess Cd ions) on the surface of the nanocrystals and 100% conversion of elemental Se into CdSe nanocrystals, the theoretical yield was 0.047 g.

3.9 Synthesis of 4 nm ZnSe nanocrystals using Se–SUS

In a typical synthesis, $ZnSt_2$ (0.0632 g, 0.1 mmol) and ODE (5 mL) were loaded into a 25 mL three-neck flask, degassed for 10 min by bubbling with argon. The temperature was then raised to 305 ˚C. In an empty vial, Se powder (0.0039 g, 0.05 mmol) was dispersed in ODE (1 mL) by sonication for 5 min and injected into the above flask. After the injection, the reaction temperature was set at 270 ˚C and the mixture annealed for 15 min. Finally, the reaction was stopped by cooling down to room temperature in air.

3.10 Synthesis of 8 nm ZnSe nanocrystals by multi-injection using Se–SUS

In a typical synthesis, $ZnSt_2$ (0.0632 g, 0.1 mmol), oleylamine (0.1 mL), and ODE (5 mL) were loaded in a 25 mL three-neck flask, and degassed for 10 min by bubbling with argon. The temperature was then raised to 240 ˚C. In an empty vial, Se powder (0.0039 g, 0.05 mmol) was dispersed in ODE (1 mL) by sonication for about 5 min and injected into the above flask. After the injection, the reaction temperature was set at 270 ˚C and maintained for 15 min. Subsequently, 0.35 mL of $ZnSt_2$ solution prepared by dissolving $ZnSt_2$ (1.896 g, 3 mmol) in ODE (10 mL) was injected into the reaction mixture. After reacting for 5 min, multiple injections with 0.1 mL of Se–SUS (0.0078 g of Se powder dispersed in 1 mL of ODE) in each injection were carried out at 5 min intervals. Aliquots (~0.05 mL) were taken for UV–vis and PL measurements to monitor the reaction. When the desired size was reached, the reaction mixture was annealed for 15 min before cooling down to room temperature in air to complete the reaction.

3.11 Synthesis of ZnSe/ZnS core/shell nanocrystals

The thermal-cycling coupled single precursor (TC-SP) method was used as the shell growth method [36]. In an empty vial, $Zn(DDTC)_2$ (0.325 g, 0.9 mmol) was dissolved in a mixture of ODE (2 mL) and oleylamine (1 mL) to form the $Zn(DDTC)_2$ solution. In a typical synthesis, 5 nm ZnSe core particles were prepared using the method mentioned above. After decreasing the reaction temperature to 80 ℃, oleylamine (0.5 mL) and TBP (0.05 mL) were added to the reaction flask, and the reaction was then held at this temperature for 10 min. At this temperature, a calculated amount of the $Zn(DDTC)_2$ solution (0.17, 0.22, 0.27, 0.32, and 0.38 mL for the 1st, 2nd, 3rd, 4th, and 5th monolayer of ZnS shell, respectively) was added dropwise into the flask. After each addition was completed, the reaction mixture was left for 5 min to allow the adsorption of $Zn(DDTC)_2$ on to the nanocrystals. For the epitaxial growth of each monolayer, the temperature was increased to 150–180 ℃. At this temperature, each growth step was allowed to proceed for 20 min, and then, the reaction solution was allowed to cool down to 80 ℃ before initiating the next cycle. After the desired thickness of shell was achieved, the reaction was stopped by cooling down to room temperature in air.

3.12 Synthesis of CdSe/ZnSe core/shell nanocrystals using Se–SUS as the Se shelling precursor

The Se–SUS was prepared by dispersing Se powder (0.0237 g, 0.3 mmol) in ODE (3 mL). The zinc formate-octylamine suspension was prepared by sonication of zinc formate (0.0465 g, 0.3 mmol) and octylamine (0.5 mL) in ODE (2.5 mL). In a typical synthesis, a mixture of oleylamine (0.5 mL), ODE (3 mL), and 1.5 mL of purified 3 nm CdSe nanocrystals solution (containing about 3×10^{-7} mol of nanocrystals estimated by their extinction coefficient [50] were loaded into a 25 mL three-neck flask. The amounts of precursor solutions for each injection were estimated using the procedure reported previously [23]. The amounts for three consecutive injections of the Se–SUS and the zinc formate–octylamine suspension were 0.15, 0.22, and 0.30 mL, respectively. After stirring and argon bubbling for 10 min, the mixture in the flask was heated to 130 ℃. At this temperature, the Se–SUS precursor of the first monolayer was injected into the reaction flask and the reaction left for 20–30 min to allow dissolution of Se powder. Then temperature was further lowered to 100 ℃ and the zinc formate–octylamine suspension for growth of the first monolayer was injected. The reaction solution was left to stir for 30 min at 100 ℃ to allow growth of the first monolayer of ZnSe. After growth of the first monolayer of the shell, the flask was heated to 130 ℃ and the Se–SUS for the second monolayer was injected and the reaction mixture kept at 130 ℃ for 20–30 min. The reaction mixture was allowed to cool down to 100 ℃ in air. At this temperature, the zinc formate–octylamine suspension for the second monolayer was injected and the reaction was kept at 100 ℃ for 10 min. Subsequently, the reaction solution was heated to 140–150 ℃ for the growth of the second monolayer of ZnSe, and the solution was kept at this temperature for 30 min for completion of the second monolayer. The synthesis of the third monolayer of ZnSe was the same as the second one except the amount of the precursors added. Needle-tip aliquots were taken and diluted in toluene for monitoring the reaction by UV–vis and PL measurements.

3.13 Synthesis of Mn:ZnSe d-dots through co-nucleation doping

In a typical synthesis, $ZnSt_2$ (0.0632 g, 0.1 mmol), $MnSt_2$ (0.0314 g, 0.05 mmol), and ODE (5 mL) were loaded into a 50 mL three-neck flask, and degassed for 10 min by bubbling with argon at 100 ℃. In an empty vial, Se powder (0.039 g, 0.5 mmol) was dispersed in ODE (0.5 mL) and oleylamine (0.5 mL) to form Se–SUS by sonication for about 5 min. Subsequently, the temperature of the mixture in the flask was increased to 290 ℃, and 1 mL of Se–SUS was injected rapidly. The reaction temperature was lowered by the injection and set at 260 ℃ for 5 min. Into this reaction mixture, 1.5 mL of the Zn stock solution (prepared by dissolving 0.75 mmol of $ZnSt_2$ and 0.75 mmol of HSt in 3 mL ODE at 100 ℃) was injected in three equal portions at 5 min interval. Finally, the remaining Zn stock solution (1.5 mL in total) was injected all at once, and the reaction mixture was annealed for 20 min at the given temperature

before cooling down to room temperature in air to stop the reaction. During the process, needle-tip aliquots were taken and diluted in toluene for monitoring the reaction by UV–vis and PL measurements.

3.14 Synthesis of the chalcopyrite phase of $CuInSe_2$

In a typical synthesis, CuAc (0.0122 g, 0.1 mmol), $InAc_3$ (0.0221 g, 0.1 mmol), oleic acid (0.5 mL), dodecanethiol (0.25 mL), and ODE (5 mL) were loaded into a 50 mL three-neck flask. The mixture was degassed at 100 ℃ by bubbling with argon for 30 min. In an empty vial, Se powder (0.0156 g, 0.2 mmol) was dispersed in ODE (1 mL) by sonication to form Se–SUS. The temperature of the mixture in the flask was increased to 180 ℃ for Se–SUS injection and growth of $CuInSe_2$ nanocrystals. Aliquots (~0.05 mL) were taken for UV–vis and PL measurements. When a precipitates was observed, the reaction temperature was allowed to cool down to room temperature in air. The precipitate was collected by centrifugation, and the precipitate obtained by decantation could be dispersed in toluene.

3.15 Synthesis of $CuInSe_2$ nanocrystals with the zinc blende structure

In a typical synthesis, CuAc (0.0122 g, 0.1 mmol), $InAc_3$ (0.0221 g 0.1 mmol), oleic acid (0.5 mL) and dodecanethiol (5 mL) were loaded into a 50 mL three-neck flask. The mixture was degassed at 100 ℃ by bubbling with argon for 30 min. At this temperature, Se–SUS (0.0156 g Se powder dispersed in 1 mL ODE) was injected into the reaction mixture. Subsequently, the temperature of the reaction mixture was increased to 150 ℃ for the further growth of $CuInSe_2$ nanocrystals. Aliquots (~0.05 mL) were taken for UV–vis and PL measurements to monitor the reaction. When desired size was reached, the reaction mixture was allowed to cool down to room temperature in air to stop the reaction.

3.16 Synthesis of $CuInSe_2$/ZnSe core/shell nanocrystals

When zinc blende $CuInSe_2$ nanocrystals with the desired size were obtained as described above, the temperature was set at 100 ℃. 1 mL of the Zn stock solution (prepared by dissolving 0.1 mmol of $ZnAc_2$ in a mixture of 0.5 mL of ODE and 0.5 mL of oleylamine) was injected into the flask. Subsequently, the reaction temperature was increased to 200 ℃ for the growth of the ZnSe shell. After 30 min of growth, the reaction mixture was cooled down to room temperature in air to stop the reaction.

3.17 Optical measurements

UV–vis spectra were recorded on an Analytik Jena S600 spectrophotometer. Photoluminescence measurements were taken on a Tianjin Gangdong F380 Fluorometer. Absolute PL QY was measured on an integrating sphere coupled with a QE65000 spectrometer from Ocean Optical Co., Ltd. Specifically, the nanocrystal samples (optical densities ~0.3) were diluted to gradient concentrations by toluene. After diluted samples reached equilibrium at room temperature, PL QY measurements were taken. For the measurements of absorbance at 320 nm of the CdSe nanocrystals (data in Fig. 2(c)), aliquots of the reaction mixture were quantitatively diluted in chloroform to avoid solvent interference.

3.18 Transmission electron microscopy

TEM images were recorded on a Hitachi 7700 microscope. Specimens were prepared by putting a drop of toluene solution containing nanocrystals (optical density ~0.3) on a copper grid coated with thin carbon film.

3.19 X-ray powder diffraction

XRD patterns were obtained using a Rigaku Ultimate-Ⅳ X-ray diffractometer operating at 40 kV/40 mA using Cu Kα radiation (λ = 1.5418 Å). Powder samples for XRD measurements were prepared by precipitation of the nanocrystals from solution using ethanol as precipitant. Precipitates collected by centrifugation and decantation were re-dissolved in toluene. The precipitation/centrifugation/decantation was repeated two more times with ethyl acetate and ethanol (1:1 in volume) as the precipitant. The final precipitates were transferred onto a glass slide for XRD measurements.

Acknowledgements

We are grateful for the financial support from the

National Natural Science Foundation of China (NSFC, No. 21233005).

Electronic Supplementary Material: Supplementary material is available in the online version of this article at http://dx.doi.org/10.1007/s12274-013-0341-7.

References

[1] Murray, C. B.; Kagan, C. R.; Bawendi, M. G. Synthesis and characterization of monodisperse nanocrystals and close-packed nanocrystal assemblies. *Annu. Rev. Mater. Sci.* **2000**, *30*, 545–610.

[2] Peng, X. G. An essay on synthetic chemistry of colloidal nanocrystals. *Nano. Res.* **2009**, *2*, 425–447.

[3] Murray, C. B.; Norris, D. J.; Bawendi, M. G. Synthesis and characterization of nearly monodisperse CdE (E = S, Se, Te) semiconductor nanocrystallites. *J. Am. Chem. Soc.* **1993**, *115*, 8706–8715.

[4] Norris, D. J.; Efros, A. L.; Erwin, S. C. Doped nanocrystals. *Science* **2008**, *319*, 1776–1779.

[5] Pradhan, N.; Goorskey, D.; Thessing, J.; Peng, X. G. An alternative of CdSe nanocrystal emitters: Pure and tunable impurity emissions in ZnSe nanocrystals. *J. Am. Chem. Soc.* **2005**, *127*, 17586–17587.

[6] Norberg, N. S.; Parks, G. L.; Salley, G. M.; Gamelin, D. R. Giant excitonic Zeeman splittings in colloidal Co^{2+}-doped ZnSe quantum dots. *J. Am. Chem. Soc.* **2006**, *128*, 13195–13203.

[7] Bussian, D. A.; Crooker, S. A.; Yin, M.; Brynda, M.; Efros, A. L.; Klimov, V. I. Tunable magnetic exchange interactions in manganese-doped inverted core–shell ZnSe–CdSe nanocrystals. *Nat. Mater.* **2009**, *8*, 35–40.

[8] Ibanez, M.; Zamani, R.; LaLonde, A.; Cadavid, D.; Li, W. H.; Shavel, A.; Arbiol, J.; Morante, J. R.; Gorsse, S.; Snyder, G. J.; Cabot, A. $Cu_2ZnGeSe_4$ nanocrystals: Synthesis and thermoelectric properties. *J. Am. Chem. Soc.* **2012**, *134*, 4060–4063.

[9] Xiao, C.; Xu, J.; Li, K.; Peng, J.; Yang, J. L.; Xie, Y. Superionic phase transition in silver chalcogenide nanocrystals realizing optimized thermoelectric performance. *J. Am. Chem. Soc.* **2012**, *134*, 4287–4293.

[10] Fan, F. J.; Wang, Y. X.; Liu, X. J.; Wu, L.; Yu, S. H. Large-scale colloidal synthesis of non-stoichiometric $Cu_2ZnSnSe_4$ nanocrystals for thermoelectric applications. *Adv. Mater.* **2012**, *24*, 6158–6163.

[11] Leschkies, K. S.; Beatty, T. J.; Kang, M. S.; Norris, D. J.; Aydil, E. S. Solar cells based on junctions between colloidal PbSe nanocrystals and thin ZnO films. *ACS Nano* **2009**, *3*, 3638–3648.

[12] Guo, Q.; Kim, S. J.; Kar, M.; Shafarman, W. N.; Birkmire, R. W.; Stach, E. A.; Agrawal, R.; Hillhouse, H. W. Development of $CuInSe_2$ nanocrystal and nanoring inks for low-cost solar cells. *Nano Lett.* **2008**, *8*, 2982–2987.

[13] Peng, Z. A.; Peng, X. G. Formation of high-quality CdTe, CdSe, and CdS nanocrystals using CdO as precursor. *J. Am. Chem. Soc.* **2001**, *123*, 183–184.

[14] Qu, L. H.; Peng, Z. A.; Peng, X. G. Alternative routes toward high quality CdSe nanocrystals. *Nano Lett.* **2001**, *1*, 333–337.

[15] Yu, W. W.; Peng, X. G. Formation of high-quality CdS and other Ⅱ–Ⅵ semiconductor nanocrystals in noncoordinating solvents: Tunable reactivity of monomers. *Angew. Chem. Int. Ed.* **2002**, *41*, 2368–2371.

[16] Deng, Z. T.; Cao, L.; Tang, F. Q.; Zou, B. S. A new route to zinc-blende CdSe nanocrystals: Mechanism and synthesis. *J. Phys. Chem. B* **2005**, *109*, 16671–16675.

[17] Yang, Y. A.; Wu, H. M.; Williams, K. R.; Cao, Y. C. Synthesis of CdSe and CdTe nanocrystals without precursor injection. *Angew. Chem. Int. Ed.* **2005**, *44*, 6712–6715.

[18] Jasieniak, J.; Bullen, C.; van Embden, J.; Mulvaney, P. Phosphine-free synthesis of CdSe nanocrystals. *J. Phys. Chem. B* **2005**, *109*, 20665–20668.

[19] Chen, O.; Chen, X.; Yang, Y. A.; Lynch, J.; Wu, H. M.; Zhuang, J. Q.; Cao, Y. C. Synthesis of metal-selenide nanocrystals using selenium dioxide as the selenium precursor. *Angew. Chem. Int. Ed.* **2008**, *47*, 8638–8641.

[20] Shen, H. B.; Niu, J. Z.; Wang, H. Z.; Li, X. M.; Li, L. S.; Chen, X. Size- and shape-controlled synthesis of ZnSe nanocrystals using SeO_2 as selenium precursor. *Dalton Trans.* **2010**, *39*, 11432–11438.

[21] Wei, Y. F.; Yang, J.; Lin, A. W. H.; Ying, J. Y. Highly reactive Se precursor for the phosphine-free synthesis of metal selenide nanocrystals. *Chem. Mater.* **2010**, *22*, 5672–5677.

[22] Liu, Y.; Yao, D.; Shen, L.; Zhang, H.; Zhang, X. D.; Yang, B. Alkylthiol-enabled Se powder dissolution in oleylamine at room temperature for the phosphine-free synthesis of copper-based quaternary selenide nanocrystals. *J. Am. Chem. Soc.* **2012**, *134*, 7207–7210.

[23] Nan, W. N.; Niu, Y. A.; Qin, H. Y.; Cui, F.; Yang, Y.; Lai, R. C.; Lin, W. Z.; Peng, X. G. Crystal structure control of zinc-blende CdSe/CdS core/shell nanocrystals: Synthesis and structure-dependent optical properties. *J. Am. Chem. Soc.* **2012**, *134*, 19685–19693.

[24] Lin, S. L.; Pradhan, N.; Wang, Y. J.; Peng, X. G. High quality ZnSe and ZnS nanocrystals formed by activating zinc carboxylate precursors. *Nano Lett.* **2004**, *4*, 2261–2264.

[25] Shen, H. B.; Wang, H. Z.; Li, X. M.; Niu, J. Z.; Wang, H.; Chen, X.; Li, L. S. Phosphine-free synthesis of high quality

ZnSe, ZnSe/ZnS, and Cu-, Mn-doped ZnSe nanocrystals. *Dalton Trans.* **2009**, *47*, 10534–10540.

[26] Liu, L. P.; Zhuang, Z. B.; Xie, T.; Wang, Y. G.; Li, J.; Peng, Q.; Li, Y. D. Shape control of CdSe nanocrystals with zinc blende structure. *J. Am. Chem. Soc.* **2009**, *131*, 16423–16429.

[27] Bullen, C.; van Embden, J.; Jasieniak, J.; Cosgriff, J. E.; Mulder, R. J.; Rizzardo, E.; Gu, M.; Raston, C. L. High activity phosphine-free selenium precursor solution for semiconductor nanocrystal growth. *Chem. Mater.* **2010**, *22*, 4135–4143.

[28] Zeng, R. S.; Rutherford, M.; Xie, R. G.; Zou, B. S.; Peng, X. G. Synthesis of highly emissive Mn-doped ZnSe nanocrystals without pyrophoric reagents. *Chem. Mater.* **2010**, *22*, 2107–2113.

[29] Yordanov, G. G.; Yoshimura, H.; Dushkin, C. D. Phosphine-free synthesis of metal chalcogenide quantum dots by means of *in situ*-generated hydrogen chalcogenides. *Colloid Polym. Sci.* **2008**, *286*, 813–817.

[30] Li, Z.; Ji, Y. J.; Xie, R. G.; Grisham, S. Y.; Peng, X. G. Correlation of CdS nanocrystal formation with elemental sulfur activation and its implication in synthetic development. *J. Am. Chem. Soc.* **2011**, *133*, 17248–17256.

[31] Rutherford, M. R. Determination of dopant ion mobility in transition metal doped semiconductor nanocrystals. Ph. D. Dissertation, University of Arkansas, Fayetteville, USA, 2010.

[32] Thessing, J.; Qian, J. H.; Chen, H. Y.; Pradhan, N.; Peng, X. G. Interparticle influence on size/size distribution evolution of nanocrystals. *J. Am. Chem. Soc.* **2007**, *129*, 2736–2737.

[33] Xie, R. G.; Li, Z.; Peng, X. G. Nucleation kinetics vs. chemical kinetics in the initial formation of semiconductor nanocrystals. *J. Am. Chem. Soc.* **2009**, *131*, 15457–15466.

[34] Capek, R. K.; Moreels, I.; Lambert, K.; De Muynck, D.; Zhao, Q.; Vantomme, A.; Vanhaecke, F.; Hens, Z. Optical properties of zincblende cadmium selenide quantum dots. *J. Phys. Chem. C* **2010**, *114*, 6371–6376.

[35] Mohamed, M. B.; Tonti, D.; Al-Salman, A.; Chemseddine, A.; Chergui, M. Synthesis of high quality zinc blende CdSe nanocrystals. *J. Phys. Chem. B* **2005**, *109*, 10533–10537.

[36] Chen, D. A.; Zhao, F.; Qi, H.; Rutherford, M.; Peng, X. G. Bright and stable purple/blue emitting CdS/ZnS core/shell nanocrystals grown by thermal cycling using a single-source precursor. *Chem. Mater.* **2010**, *22*, 1437–1444.

[37] Reiss, P.; Bleuse, J.; Pron, A. Highly luminescent CdSe/ZnSe core/shell nanocrystals of low size dispersion. *Nano Lett.* **2002**, *2*, 781–784.

[38] Battaglia, D.; Li, J. J.; Wang, Y. J.; Peng, X. G. Colloidal two-dimensional systems: CdSe quantum shells and wells. *Angew. Chem. Int. Ed.* **2003**, *42*, 5035–5039.

[39] Kim, S.; Lim, Y. T.; Soltesz, E. G.; De Grand, A. M.; Lee, J.; Nakayama, A.; Parker, J. A.; Mihaljevic, T.; Laurence, R. G.; Dor, D. M.; et al. Near-infrared fluorescent type Ⅱ quantum dots for sentinel lymph node mapping. *Nat. Biotechnol.* **2004**, *22*, 93–97.

[40] Blackman, B.; Battaglia, D.; Peng, X. G. Bright and water-soluble near IR-emitting CdSe/CdTe/ZnSe Type-Ⅱ/Type-Ⅰ nanocrystals, tuning the efficiency and stability by growth. *Chem. Mater.* **2008**, *20*, 4847–4853.

[41] Zhong, X. H.; Feng, Y. Y.; Zhang, Y. L.; Gu, Z. Y.; Zou, L. A facile route to violet- to orange-emitting $Cd_xZn_{1-x}Se$ alloy nanocrystals via cation exchange reaction. *Nanotechnology* **2007**, *18*, 385606.

[42] Pradhan, N.; Peng, X. G. Efficient and color-tunable Mn-doped ZnSe nanocrystal emitters: Control of optical performance via greener synthetic chemistry. *J. Am. Chem. Soc.* **2007**, *129*, 3339–3347.

[43] Pradhan, N.; Battaglia, D. M.; Liu, Y. C.; Peng, X. G. Efficient, stable, small, and water-soluble doped ZnSe nanocrystal emitters as non-cadmium biomedical labels. *Nano Lett.* **2007**, *7*, 312–317.

[44] Chen, D. A.; Viswanatha, R.; Ong, G. L.; Xie, R. G.; Balasubramaninan, M.; Peng, X. G. Temperature dependence of "elementary processes" in doping semiconductor nanocrystals. *J. Am. Chem. Soc.* **2009**, *131*, 9333–9339.

[45] Pan, D. C.; An, L. J.; Sun, Z. M.; Hou, W.; Yang, Y.; Yang, Z. Z.; Lu, Y. F. Synthesis of Cu–In–S ternary nanocrystals with tunable structure and composition. *J. Am. Chem. Soc.* **2008**, *130*, 5620–5621.

[46] Connor, S. T.; Hsu, C. M.; Weil, B. D.; Aloni, S.; Cui, Y. Phase transformation of biphasic Cu_2S–$CuInS_2$ to monophasic $CuInS_2$ nanorods. *J. Am. Chem. Soc.* **2009**, *131*, 4962–4966.

[47] Xie, R. G.; Rutherford, M.; Peng, X. G. Formation of high-quality Ⅰ–Ⅲ–Ⅵ semiconductor nanocrystals by tuning relative reactivity of cationic precursors. *J. Am. Chem. Soc.* **2009**, *131*, 5691–5697.

[48] Li, L. A.; Pandey, A.; Werder, D. J.; Khanal, B. P.; Pietryga, J. M.; Klimov, V. I. Efficient synthesis of highly luminescent copper indium sulfide-based core/shell nanocrystals with surprisingly long-lived emission. *J. Am. Chem. Soc.* **2011**, *133*, 1176–1179.

[49] Kar, M.; Agrawal, R.; Hillhouse, H. W. Formation pathway of $CuInSe_2$ nanocrystals for solar cells. *J. Am. Chem. Soc.* **2011**, *133*, 17239–17247.

[50] Yu, W. W.; Qu, L. H.; Guo, W. Z.; Peng, X. G. Experimental determination of the extinction coefficient of CdTe, CdSe, and CdS nanocrystals. *Chem. Mater.* **2003**, *15*, 2854–2860.